JOURNAL OF MATERIALS SCIENCE 26 (1991) 3853–3861

Effects of boron and heat treatment on structure of dual-phase Ti–TiC

R. ZEE, CHI YANG, YIXING LIN, B. CHIN
Materials Engineering, Auburn University, Auburn, AL 36849, USA

An *in situ* method was developed to fabricate a two-phase mixture of titanium carbide in a titanium matrix by solidification from a titanium–carbon melt. The solidified morphology consisted of three-dimensional TiC dendrites in a titanium matrix. The secondary dendrite arm spacing was found to be influenced by the presence of boron. The structure and microhardness of the components as a function of boron content and heat-treatment procedure were determined. Heat treatment plays a major role in the structure while the effect of boron is minimal. Results from X-ray diffraction analysis indicate that the solidified carbide is very rich in vacancies in the carbon sublattice. Annealing leads to a redistribution of the titanium atoms to occupy some of the vacant carbon sites. This thermal redistribution effect results in a dramatic decrease in the hardness of the carbides. The lattice parameter measurement supports the above structure evolution.

1. Introduction

Titanium-based alloys have received increasing attention due to their high strength-to-weight ratio and high-temperature properties. However, to extend the usefulness of these materials, composites with high strength and lightweight reinforcements have been extensively studied. Most of these investigations centred on consolidating the matrix material and the reinforcement together via various techniques, the most common of which are solid-state sintering, liquid infiltration and plasma spraying. In this study, an *in situ* method was used to produce a hybrid mixture of three-dimensional TiC reinforcement in a titanium matrix. This ceramic–metal combination is similar to cermets. However, the *in situ* solidification of the carbide provides morphological control of the structure. Addition of carbon to titanium produces a dual-phase material (α-Ti and TiC) by exceeding the solid solubility of carbon in titanium. This hybrid material is composed of a high-strength but rather brittle TiC phase which is embedded in a ductile titanium matrix. The concept of combining the advantages of both metal and ceramics in metal-matrix composites seems successful for this material. The TiC phase is ordered and thus possesses the advantages similar to long-range ordered (LRO) alloys. The atomic ordering produces a pronounced increase in the work-hardening [1–3], improves the fatigue resistance [4] and retards, because of stronger binding and closer packing of atoms, most thermally activated processes such as creep and grain growth [5]. In addition, the strength of entirely ordered alloys is less sensitive to temperature than that of conventional disordered alloys. In fact some ordered alloys show an increase rather than a decrease in strength with increasing temperature up to the critical ordering point. The objective of this study is to investigate the effects of boron addition and heat treatment on the structure of the ordered TiC and the titanium matrix. The atomic diameter of boron is slightly larger than that of carbon. It is conceivable that boron substitutes for carbon in TiC. Boron additions to titanium have been found to decorate the solidification interfaces of Ti alloys, hence improving the tensile and yield strength. However, the formation of Ti–B compounds along the α-grain boundaries decreases the ductility.

Traditional ingot metallurgy plus solidification techniques were used to produce Ti–TiC metal-matrix composites. These approaches have advantages such as producing fully dense ceramic materials, controlling the size and shape of the reinforcements, obtaining three-dimensional reinforcements and manipulating the degree of order in the structure.

2. Experimental procedure

A series of Ti–TiC materials, with and without boron additions, were produced by induction melting. Boron was added either in the elemental form or as TiB_2. The set-up of the melting process and the nominal compositions of samples fabricated are shown in Fig. 1. Blended graphite and TiB_2 or boron powder was packed into holes drilled in titanium rods and then placed into graphite crucibles. Tantalum foil (the susceptor material) was wrapped around the crucible inside the quartz tube to evenly heat the sample by induction. The melting was performed using a 5 kW induction generator. An argon atmosphere was employed to prevent oxidation. An ultrasonic vibrator was used to promote stirring of the melt. The crucible was dropped into water for quenching after holding

0022–2461/91 $03.00 + .12

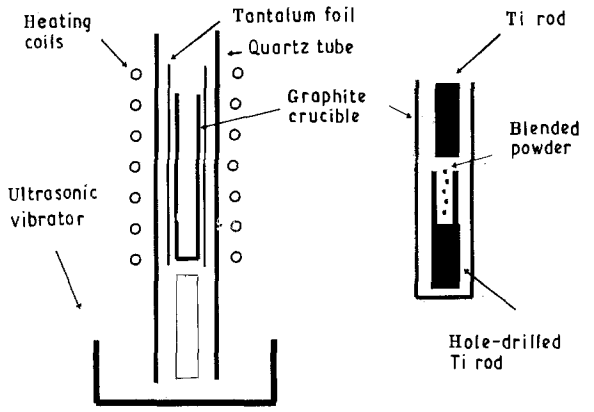

Figure 1 Experimental set-up for the melting process.

for 1 min in the molten state. The final size of the ingot obtained was 9.5 mm in diameter and 32 mm high.

Quantitative image analysis was done with a Zeiss microscope and a Microcomp image analysis system (Model No. NC-655). Since carbon was absorbed from the graphite crucible during the melting process, the volume fraction of the carbide phase was used instead of nominal compositions to specify the alloy. The value derived was determined by six measurements made from top to bottom of each specimen, cut through the longitudinal direction of the as-quenched ingot. Secondary dendrite arm spacing (SDAS) was also measured for each specimen. The boron distribution over the as-quenched samples was determined by Auger electron spectroscopy (AES). The Auger peaks of the individual elements were analysed using a high-transmission scanning Auger microprobe (XSAM-800). The specimens were cut directly from the as-quenched samples and then mounted on the sample holder, using silver paint to obtain good electrical conductivity. Prior to measurement, the specimens were cleaned and heated to remove moisture and hydrocarbon. Scans with and without argon ion bombardment were performed to reveal the influence of hydrocarbon on the peak area of Auger electron peaks.

Both bulk specimens and extracted TiC powder were examined using X-ray diffractometry (XRD). A Rigaku D/MAXB X-ray diffractometer was used to analyse the specimens with copper radiation. Bulk samples were prepared by cutting directly from the as-quenched ingots along a longitudinal direction. A scan speed of 5 or 10° min^{-1} was used. The lattice parameters of titanium were calculated from the d spacings. Powder samples of TiC were prepared by dissolving the titanium matrix out of the as-quenched ingots with a solution composed of water, nitric acid and hydrofluoric acid in proportions of 45:4:1. TiC powder purchased from Johnson Matthey Co. was also analysed to serve as a reference. The lattice parameter and degree of long-range order (S) of TiC were calculated after measurement. For calculating the degree of long-range order, a scan speed of 0.5° min^{-1} was used to obtain optimal resolution. Purchased and extracted TiC powders were heat-treated by a turbo-molecular vacuum furnace for 8 h at 1273 K and 18 h at 1637 K separately, then furnace cooled to room temperature. These heat-treated samples were also analysed using X-ray diffractometry. The lattice parameters and S were calculated from these measurements.

A Leco DM-400 hardness tester was used to determine the microhardness of the individual phases. The microhardness in VHN was obtained after 100 g standard load indentation with 5 s indentation time. All measurements were done at room temperature and the values reported are the average of ten individual data points.

3. Results

3.1. Microstructure

Fig. 2a to c show the microstructure of the Ti–TiC material without boron addition, with B addition in the elemental form, and with B addition in the TiB_2 form, respectively. All three systems contained both titanium matrix and TiC dendrite particles. This was further confirmed by microhardness results for individual phases and X-ray results, which will be shown later.

From image analysis, the volume fraction of the dendritic TiC was found to range from 31 to 44% for the samples with or without boron addition. The presence of boron, in either the elemental or the boride form, reduced the size of the dendrite particles. The SDAS of the TiC phase was also obtained using image analysis, and it showed a decrease with increasing boron content as shown in Table I. This implies that boron additions refine the TiC microstructure in the Ti–TiC material.

Boron distribution in the Ti–TiC materials was analysed using AES. Fig. 3a and b show the typical AES spectra of boron addition samples without and with ion-sputtering for 14 min, respectively. Boron peaks existed in both spectra, which provided direct evidence that boron did enter the Ti–TiC system after solidification. It was also found that the peak-to-peak heights of carbon were reduced and that of boron increased after ion-bombardment removal.

3.2. Structure determination by XRD

The as-quenched samples were cut along the longitudinal direction and then analysed by X-ray diffractometer. Pure titanium was also analysed to serve as a standard. Fig. 4 shows the typical X-ray spectrum of a solidified sample. Titanium and TiC were the only two components identified in all the solidified samples. This implies that the TiB_2 powder, elemental boron and free graphite were all dissolved in the molten titanium during the melting process. Peak shifts, as compared with pure titanium, were observed in all the samples.

Alpha-titanium has an h.c.p. structure. To calculate the lattice parameters of the α-titanium phase, a modified Massalski's method [6] was used. The modification involved a computer analysis instead of the tradi-

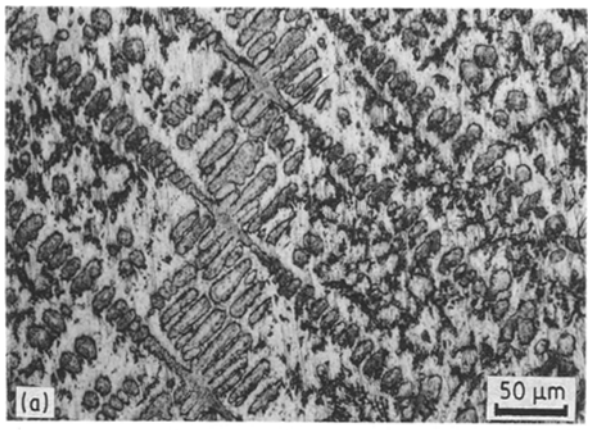

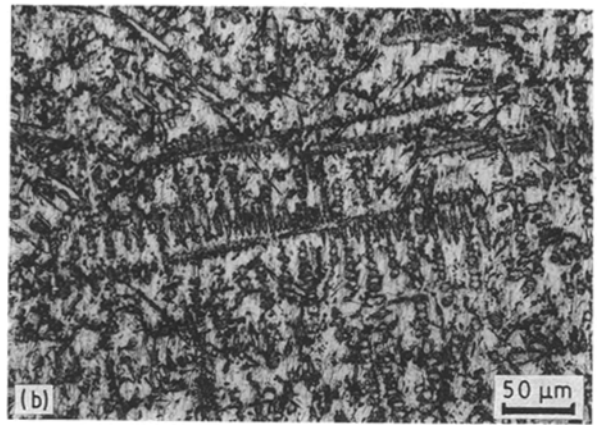

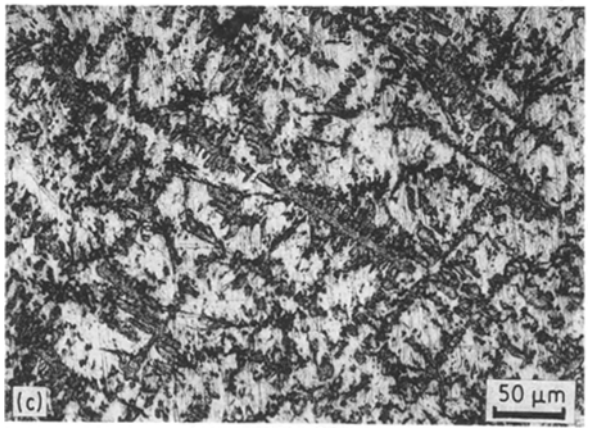

Figure 2 Microstructure of Ti–TiC system (a) without boron addition, (b) with boron added in the elemental form and (c) with boron added in the boride form.

TABLE I Results of image analysis

Nominal composition	Volume fraction (%)	SDAS (μm)
1C–Ti	31	11.2
0.5B–1C–Ti (B)	39	7.1
1B–1C–Ti (B)	31	6.6
0.5B–1C–Ti (TiB_2)	44	7.2
1B–1C–Ti (TiB_2)	36	6.8

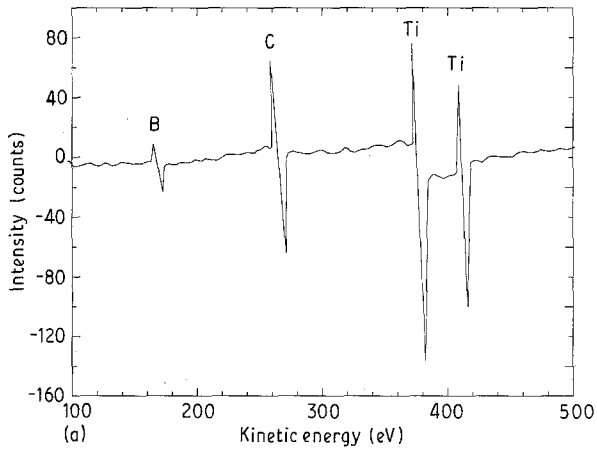

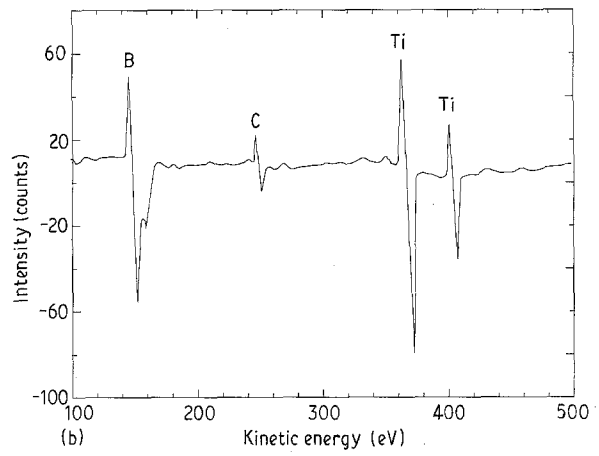

Figure 3 Typical AES spectra of TiC with boron addition taken (a) before ion-bombardment and (b) after ion-bombardment for 14 min.

tional graphical method. A computer program to perform the calculation was developed. Precise values of a_0 and c_0 were determined by extrapolating the values from each peak to the limit of $\cos^2\theta/\sin\theta = 0$. The lattice parameters of pure titanium and solidified samples are given in Table II. It can be seen that carbon expands the titanium unit cell by increasing both the a_0 and the c_0 constants. Additions of boron to the Ti–TiC system in the elemental or the boride forms expanded the titanium lattice further, but to a lesser extent.

Purchased TiC powder was first scanned by XRD to serve as a standard. For solidified samples, TiC powder was obtained by dissolving the titanium matrix out of the as-quenched ingots. Fig. 5 shows the morphology of the extracted TiC powder. Most of the powder exists in the dendrite form which is identical with the features shown in optical micrographs. The TiC powder extracted from solidified samples was examined by XRD. A typical X-ray spectrum from the extracted TiC is shown in Fig. 6. These values for the TiC structure are given in Table III. For solidified samples, the lattice constant, a_0, of TiC always showed a decrease as compared to that of the TiC-standard.

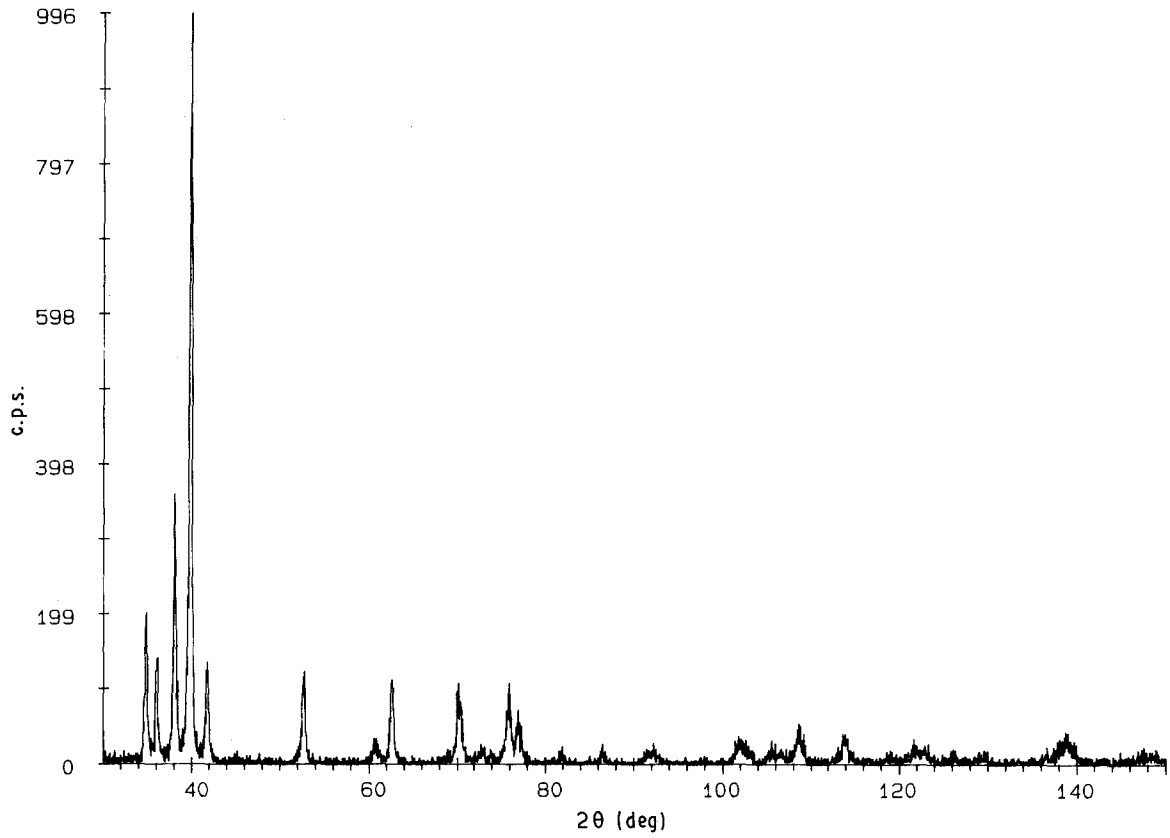

Figure 4 Typical X-ray spectrum of a solidified Ti–TiC sample in the bulk form containing a two-phase mixture of Ti and TiC with boron addition.

TABLE II Lattice parameters of α-titanium

Specimen	Lattice constants (nm)	
	a_0	c_0
Ti-standard	0.294809	0.467045
1C–Ti	0.295519	0.469396
0.5B–1C–Ti (B)	0.295662	0.468193
1B–1C–Ti (B)	0.295760	0.469625
0.5B–1C–Ti (TiB_2)	0.295681	0.469075
1B–1C–Ti (TiB_2)	0.295970	0.468167

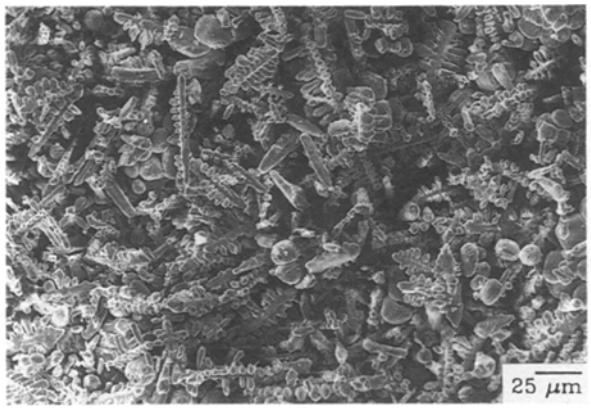

Figure 5 SEM micrograph of extracted TiC powder.

To determine whether the structure was thermodynamically stable, the TiC standard was heat-treated at 1273 K for 8 h and 1673 K for 18 h separately. These samples were then analysed by XRD. The results, also shown in Table III, reveal that decreases in lattice constant are smaller than those of solidified samples. This implies that the TiC powder as purchased has a more stable structure. Two solidified samples were also heat-treated at 1273 K for 8 h. The results show that a_0 increases with heat treatment. A metastable TiC phase is produced during the water-quenching process and becomes stable after annealing.

Besides the lattice parameter, XRD was also used to determine S, the degree of long-range order, of the TiC produced. Normally, one would use the following relationship to compute S:

$$S^2 = \frac{(I_s/I_f)_{\text{measured}}}{(I_s/I_f)_{S=1,\text{measured}}} \quad (1)$$

where I is the measured intensity and subscripts s and f represent superlattice and fundamental lines, respectively. However, in this case it is impossible to obtain perfectly ordered ($S = 1$) TiC as a reference. Therefore the quantity $(I_s/I_f)_{S=1,\text{measured}}$ cannot be experimentally determined. Instead, this value was calculated based on the equation

$$I = F^2 p \left(\frac{1+\cos^2 2\theta}{\sin^2\theta\cos\theta}\right) e^{-2M} \quad (2)$$

where p is the multiplicity factor, θ is the Bragg angle and the exponential term is the temperature factor. The structure factor, F, is a function of the atomic scattering factors f_{Ti} and f_C. For the TiC structure

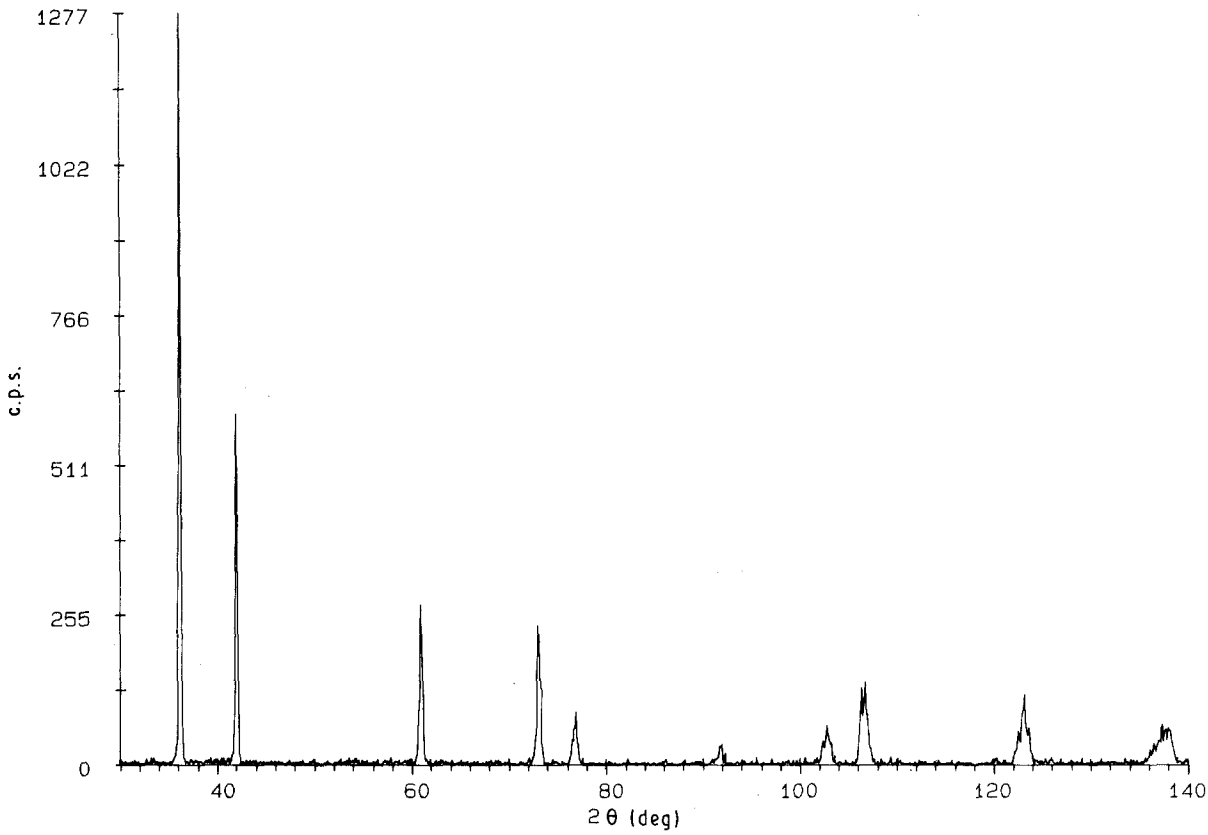

Figure 6 Typical X-ray spectrum taken from extracted TiC particles.

TABLE III Lattice parameter of TiC

Specimen	a_0 (nm)
TiC–standard	0.43283
1C–Ti	0.43129
0.5B–1C–Ti (B)	0.43049
1B–1C–Ti (B)	0.43024
0.5B–1C–Ti (TiB_2)	0.43065
1B–1C–Ti (TiB_2)	0.42942
TiC standard (HT, 1273 K, 8 h)	0.43278
TiC standard (HT, 1673 K, 18 h)	0.43266
1C–Ti (HT–1273 K, 8 h)	0.43150
0.5B–1C–Ti (B) (HT, 1673 K, 8 h)	0.43246

TABLE IV Results for intensity ratio and degree of long-range order (S) of TiC from X-ray diffraction

Specimen	$I_{(1\,1\,1)}/I_{(2\,2\,2)}$	S
$(TiC)_{S=1,\,calculated}$	5.36	1.00
TiC standard	4.27	0.90
1C–Ti	9.13	1.30
0.5B–1C–Ti (B)	10.95	1.42
1B–1C–Ti (B)	8.27	1.24
0.5B–1C–Ti (TiB_2)	7.98	1.22
1B–1C–Ti (TiB_2)	8.08	1.23
TiC standard (HT, 1273 K, 8 h)	4.86	0.95
TiC standard (HT, 1673 K, 18 h)	4.35	0.90
1C–Ti (HT, 1273 K, 8 h)	3.99	0.86
0.5B–1C–Ti (B) (HT, 1673 K, 8 h)	4.28	0.89

$$F = 4(f_{Ti} + f_C) \quad \text{for even } hkl \tag{3}$$

$$F = 4(f_{Ti} - f_C)S \quad \text{for odd } hkl \tag{4}$$

All mixed combinations of hkl values result in vanishing F. The atomic scattering factors were acquired from MacGillary and Rieck [7].

Initially, the measured intensities of superlattice and fundamental lines selected were $I_{(1\,1\,1)}$ and $I_{(2\,0\,0)}$ which are the first and the second peaks present in the X-ray spectra and are the two most intense lines. However, the ratios $I_{(1\,1\,1)}/I_{(2\,0\,0)}$ obtained were found to be inconsistent from one scan to another for the solidified samples. This inconsistency is due to the preferred orientation and morphology of the extracted TiC powder. To obtain more meaningful intensity ratios, the physical packing effect must be eliminated. There is another fundamental line (2 2 2) that exists in the X-ray spectra which belongs to the same family as the superlattice line (1 1 1). Hence the (2 2 2) peak can be used to eliminate any preferred orientation effect. When this was done, the results were found to be consistent from scan to scan. The intensity ratios $I_{(1\,1\,1)}/I_{(2\,2\,2)}$ and S are given in Table IV. A lower scan speed of 0.5° min^{-1} was used as compared to that used to determine lattice parameters (5° min^{-1}). This was done to obtain better resolution and hence more precise intensity ratios. This is especially important

since the intensity of the (2 2 2) lines can be quite weak.

From Table IV, it can be seen that the purchased TiC standard has a near-perfect long-range order (S), and heat treatment of the sample does not significantly alter S. Solidified samples have significantly higher values of S ranging from 1.22 to 1.42. It is physically impossible to have an order greater than unity. The large values of S obtained are direct evidence for the presence of vacancy defects in the carbon sublattice. This will be discussed in the next section. Heat treatment decreases the apparent order parameter S of the solidified samples back to near-unity values similar to that of the TiC standard. This similarity (between the solidified samples and the TiC standard) has to be viewed as coincidental, since the composition of the TiC standard is near to stoichiometry whereas the solidified samples are deficient in carbon. The decrease in the apparent order S after heat treatment of the solidified samples is a result of the metastable nature of the TiC structure obtained by solidification.

TABLE V Results of microhardness testing

Specimen[a]	Microhardness (VHN)	
	Ti matrix	TiC particles
1C–Ti (slow cool)	220 ± 26	600 ± 84
1C–Ti (fast cool)	203 ± 29	1418 ± 272
0.5B–1C–Ti (B)	223 ± 17	1502 ± 295
1B–1C–Ti (B)	222 ± 26	1608 ± 388
0.5B–1C–Ti (TiB_2)	234 ± 14	1536 ± 252
1B–1C–Ti (TiB_2)	260 ± 30	1540 ± 252
1C–Ti (fast cool) (HT, 1273 K, 8 h)	266 ± 41	985 ± 280
0.5B–1C–Ti (B) (HT, 1273 K, 8 h)	229 ± 16	852 ± 186
1B–1C–Ti (B) (HT, 1273 K, 8 h)	287 ± 40	983 ± 339
0.5B–1C–Ti (TiB_2) (HT, 1273 K, 8 h)	266 ± 21	949 ± 181
1B–1C–Ti (TiB_2) (HT, 1273 K, 8 h)	264 ± 19	880 ± 164

[a] All specimens are fast-cooled except the first one which is slow-cooled as indicated.

3.3. Microhardness

The results of microhardness testing are shown in Table V. All but one specimen were obtained by quenching the molten ingot in water. One specimen, without boron, was obtained by slow cooling at a rate of approximately 100 °C min^{-1}. This specimen is included to illustrate the dramatic effect of cooling rate. Rapid cooling (by quenching into water) resulted in a 1.5-fold increase in the hardness of the TiC phase with a small reduction in the matrix. Addition of boron either in the elemental form or in the boride form increased the microhardness of both Ti matrix and TiC particles. The amount of increase is approximately proportional to the boron content. Therefore, it is plausible to assume that boron enters the restricted interstitial solid solution in the Ti matrix and substitutes for carbon vacancy sites in the TiC particles. These produce strengthening effects by solution-strengthening of the titanium and by changing the structure of TiC, respectively. Fig. 7a to c show the pyramids caused by indentation during microhardness testing. It is apparent that there are cracks pro-

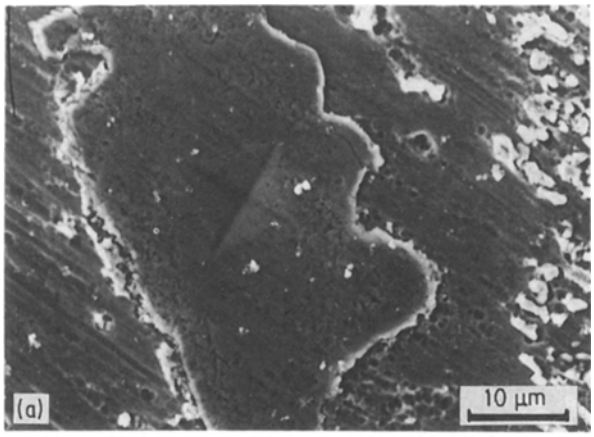

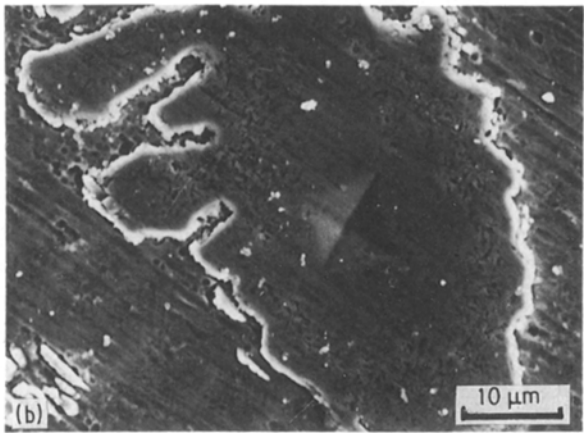

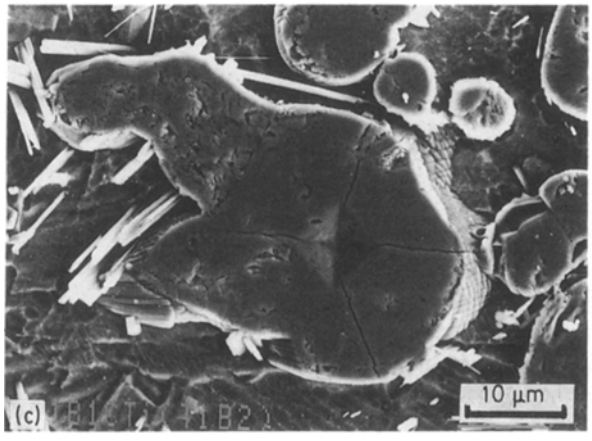

Figure 7 Pyramid generated by hardness indentation for the Ti–TiC material (a) without boron addition, (b) with boron added in the elemental form and (c) with boron added in the boride form. Note that only (c) contains cracks due to the brittle nature.

pagating along the tips of the pyramid for boron-containing samples with the boron introduced in the TiB_2 form. No cracks could be found for the Ti–TiC system with boron added in the elemental form. This indicates that addition of boron in the boride form produces brittle TiC as compared with the system with boron added in the elemental form and the system without boron.

Annealing the as-cast materials resulted in a small increase in the hardness of the matrix and a large reduction of hardness in the TiC particles. The annealing condition in terms of diffusion distance does not permit gross redistribution of composition. The observed effect in the matrix is likely to be the absorption of oxygen and nitrogen into the materials, which is known to harden titanium. The reduction of hardness in TiC is a consequence of a change in the defect state due to annealing. This observation is in accord with the change in apparent order detected in the XRD experiment and will be discussed in detail in the following section.

4. Discussion

In general, microstructural refinement of titanium alloys can be attained through rapid quenching. Furthermore, small amounts of an additive element such as metalloid constituents can alter microstructural characteristics of the as-quenched state. Such additive elements exist in the as-quenched state either in the form of a supersaturated solid solution or in the form of a solute cluster [8]. It has been well established that microstructural features such as dendrite arm spacing, grain size and second-phase inclusion size are exponential functions of the average cooling rate. Any enhancement of the mechanical properties is a consequence of the combined effects of one or more of the microstructural refinements. For the Ti–TiC systems studied, it can be seen from the results of image analysis that both the dendrite size and the secondary dendrite arm spacing of TiC are refined by boron addition. Also, increasing the boron content produces finer spacings. This phenomenon is the same as that of many alloy systems. Bower and Randlett [9] have proposed an equation for copper–silver alloys

$$d = 306R^{-0.39}C^{-0.31} \quad (5)$$

where d is the dendrite arm spacing in microns, R is the cooling rate in degrees celsius per minute, and C is the silver content in atomic per cent. An equation of this form seems to agree well for Ti–TiC systems with boron additions. In this research, the melting and the quenching processes were the same, hence the cooling rate was assumed to be fixed for the three systems produced (Ti–TiC systems without boron additions, with boron additions in the form of elemental boron and in the form of TiB_2 separately). Therefore, addition of boron to the Ti–TiC systems become the only factor that refined the size of the dendrite and the SDAS of dendritic TiC.

In recent years, titanium alloys have been routinely processed by rapid solidification techniques with cooling rates in the range of 10^5–10^7 K s^{-1}. This extremely high cooling rate can extend the solubility of boron in α-titanium from 0.55 at % for normal solidification to 10 at % for rapid solidification [10]. In the present study, the cooling rate was qualitatively estimated to be around 10^2 K s^{-1} which lies between that of normal solidification and rapid solidification. Hence the solubility of boron in α-titanium for Ti–TiC systems was suspected to be higher than 0.55 at %. The diameter ratio of boron to titanium, 0.66, is higher than the upper limit of 0.59 suggested by Hagg [11] for interstitial solid-solution alloying. However, from the XRD results, the unit cell of titanium was expanded by boron addition and expanded further with increasing boron content. This suggests that boron atoms do form an interstitial solid solution with titanium, which results from the water-quenching process after the molten state. This conclusion is further confirmed by the fact that the microhardness of the Ti matrix is increased with increasing boron content as shown in Table V. Solute atoms, such as carbon and boron, expand the unit cell of titanium and produce stress fields around these atoms which strengthen the titanium matrix.

The long-range order parameter (S) of TiC derived from the XRD results is shown in Table IV. These results show that boron additions have little effect on the degree of order. The TiC standard used is in the form of powder and of near-exact stoichiometry. The measured intensity ratios of these materials, both in the as-received and the annealing conditions, yield near-unity S values based on the computed ratio for perfect order, indicating the validity of the order calculation. The small increase in order due to annealing is a result of the ordering process both at 1273 K and during slow cooling.

The important parameters controlling the apparent S are the solidification and the annealing conditions. The TiC produced by quench solidification has an apparent order parameter larger than unity. These large values can either be attributed to an incorrect reference for perfect order or to defect states which can lead to a modification of the intensity ratio of the (1 1 1) superlattice reflection to the (2 2 2) fundamental. The former implies firstly that stoichiometric TiC (the TiC standard) has a degree of order of at most 0.6, and secondly that the solidified TiC (which is deficient in carbon) has a higher degree of order than stoichiometric TiC. Both conditions are improbable if not impossible. One factor that could have influenced the calculation of S is the dendritic morphology of TiC. In our first attempt to determine S, measured intensities of the superlattice line and fundamental line selected were respectively $I_{(1\,1\,1)}$ and $I_{(2\,0\,0)}$, which were the two most intense lines present in the X-ray spectra. For the solidified dendritic TiC, values of the $I_{(1\,1\,1)}/I_{(2\,0\,0)}$ ratio were found to vary from scan to scan. Another fundamental line (2 2 2), which is of the same family as the superlattice line (1 1 1), was used thus eliminating all preferred orientation effects.

According to the Ti–C phase diagram, TiC exists over a large range of stoichiometry from $TiC_{0.5}$ to

TiC. From the study of Kerans *et al.* [12], TiC_{1-X} varies in composition from 33 to 49 at % C at room temperature. There is substantial deviation of stoichiometry in carbon-poor compositions but none in carbon-rich compositions. It has been demonstrated that the governing thermodynamics will not permit a situation in which the phase contains more carbon atoms than titanium atoms [12]. The solidified samples should have a $TiC_{0.5}$ composition. Previous studies have suggested that in this carbon-deficient structure, the titanium sublattice is relatively perfect, whereas the carbon sublattice is only partially filled. The values of S were obtained using the intensity ratio of the (1 1 1) superlattice reflection to the (2 2 2) fundamental. The basic calculations only consider the arrangement of the titanium atoms and carbon atoms without including any lattice defects. This is normally acceptable since defect concentrations are usually quite small. However, this is not the case in substoichiometric TiC. The presence of vacancies in the carbon sublattice can be accounted for by an average f_C value which is based on the fractional occupation of the carbon sublattice by the carbon atoms. To a first approximation, it is reasonable to use an atomic scattering factor of zero for vacancies. This of course assumes the electron density in a carbon vacancy to be zero, which implies that there is no relaxation of the titanium electron distribution into the vacant sites. Based on this assumption, an intensity ratio of 8.2 is obtained for the $TiC_{0.5}$ structure with a corresponding apparent order of 1.24. This value compares favourably with those observed in the solidified samples and therefore confirms the high vacancy structure (50% occupation probability for the carbon sublattice) of the substoichiometric TiC.

Upon annealing at 1273 K for 8 h, the apparent order of the solidified carbides was reduced to approximately 0.9. This reduction is most likely due to the rearrangement of the structure to a more thermal equilibrium condition. The temperature and time of the annealing do not permit long-range redistribution of the species and a constant composition can be assumed. During annealing of the solidified carbides, the titanium atoms in the structure migrate into the vacant sites of the carbon sublattice. The process leads to a state where the carbon sublattice is now partitioned between carbon atoms, titanium atoms and vacancies whereas the titanium sublattice is still relatively free of defects. This structure can be mathematically accounted for again by a weighted average of the atomic scattering factors for the carbon sublattice, f_C. Using the measured intensity ratio of 4 for the annealed materials, this simple partition assumption of the carbon sublattice leads to occupation probabilities of 0.5, 0.3 and 0.2 for carbon, vacancy and titanium, respectively. A direct comparison of these X-ray results with the microhardness data shows that this atomic rearrangement of the structure leads to lower hardness values, indicative of the weakening effects due to this redistribution process. Furthermore, these results also illustrate that the solidified TiC has a metastable structure which becomes stable by annealing.

The order-parameter study is in agreement with the results from the lattice-parameter measurements. As shown in Table III, the unit cell of the TiC phase is reduced by quench solidification compared to the stoichiometric TiC. Earlier studies demonstrated that carbon deficiency was accompanied by a shrinkage in the unit cell in accord with our observation. The carbide lattice also expands slightly upon annealing due to the redistribution of the titanium atoms into the carbon sublattice.

5. Conclusions

The effects of boron and heat treatment on the structure and properties of Ti–TiC materials produced by solidification were investigated and the results can be summarized as follows:

1. The secondary dendrite arm spacing (SDAS) of dendritic TiC was decreased by boron additions. The SDAS was further decreased by increasing boron content.
2. The presence of boron and carbon increases the lattice size of the α-titanium matrix, consistent with the interstitial nature of these two elements.
3. The degree of long-range order (S) for the TiC structure must be interpreted with care due to the presence of carbon vacancies. Results are consistent with the condition that the as-solidified carbides contain large concentrations of vacancies in the carbon sublattice, which leads to large apparent values of the order parameter. Annealing resulted in a reduction of the apparent order parameter due to the redistribution of titanium atoms.
4. Results from the order parameter, lattice parameter and hardness analyses are consistent with one another in terms of the defect structure of the substoichiometric TiC phase and the metastable nature of the TiC produced by the solidification process.

Acknowledgements

This work was supported by the US Air Force Office of Scientific Research under grant No. AFOSR-88-0036. We would like to thank the United States Air Force for financial support.

References

1. F. MUTO and Y. TAKAGI, "The Theory of Order-Disorder Transformations in Alloys" (Academic, New York, 1956).
2. L. E. POPOV and N. A. KONEVA, in "Order Disorder Transformations in Alloys", edited by J. Warlimont (Springer, New York, 1974) p. 404.
3. M. J. MARCINKOWSKI, *ibid.* p. 364.
4. R. C. BOETLNER, N. S. STOLOFF and R. G. DAVIS, *Trans. AIME* **236** (1966) 131.
5. E. M. SCHULSON, *J. Nucl. Mater.* **66** (1977) 322.
6. T. B. MASSALSKI and H. W. KING, *J. Inst. Metals* **89** (1961) 169.
7. C. H. MacGILLARY and G. D. RIECK (eds), "International Tables for X-Ray Crystallography", Vol. 3 (Kynoch, Birmingham, 1962).
8. S. H. WHANG, *J. Metals* (April 1984) 34.

9. T. F. BOWER and M. R. RANDLETT, in "Metals Handbook", Vol. 9, 9th Edn (ASM, Metals Park, 1986) pp. 637–645.
10. S. H. WHANG and C. S. CHI, in "Rapidly Solidified Alloys and Their Magnetic Properties", edited by B. C. Giessen, MRS Symposium Proceedings Vol. 58 (1986) pp. 353–359.
11. G. HAGG, *Z. Phys. Chem.* **63** (1929) 221.
12. R. J. KERANS, K. S. MAZDIYASNI, R. RUH and H. A. LIPSITT, *J. Amer. Ceram. Soc.* **67** (1984) 34.

Received 10 April
and accepted 19 November 1990